OPTIMAL DESIGN AND CONTROL OF ELECTRIC VEHICLE POWER CHAIN

A. BELGACEM, M. A. FAKHFAKH and S. TOUNSI
National School of Electronics and Telecommunications of Sfax-Sfax University
Sciences and Technologies of image and Telecommunications Research Unit
Pôle technologique, Route de Tunis Km 10,
B.P. 1163, 3018 Sfax-Tunisie
Tél. : 74 863 047, 74 862 500 – Fax : 74 863 037

Abstract: *In this paper, a methodology of scalar control of electric cars power chain is described .This methodology takes into account of system interactions .This type of control is suitable for converter with electromagnetic switches. This choice of this converter is in order to push the multiple disadvantages of the IGBTs converters and especially to reduce the cost of global power chain. The overall model of the power chain implanted under Matlab-Simulink simulation environment leads to results of very good standard.*

Key words: *Electric vehicle, Optimal control, Design, Systemic, Electric motor, Electromagnetic converter.*

1. Introduction

In this paper, we present a systemic scalar control and design method of electric vehicle (EVs) power chain , taking into account several constraints such as the speed limit, the energy saving, the cost of the power chain and the reliability of the whole system. This method is based firstly on the analytical sizing of the power chain, and secondly on the analytical modeling of the controll parameters of the electric actuator [1], [2], [3], [4], [5], [6]. It takes into account the compatibility between the components of the power chain to reach the critical level of performance of the global system. This approach is based on the application of the general theorems relating to the design of electrotechnical devices [7], [8], [9]. The global design model provides results relating to the manufacturing of the electric motor, converter and the mechanical transmission system [1], [2], [3]. These results increases the compatibility of this approach with the optimization procedures of EVs performance such as the speed limit, the autonomy, the production cost etc [1]. This study ends with a validation study of the design approach. Indeed, the simulation of the electrical, mechanical and magnetic behavior on a global control model of this chain fully validates the design approach.

2. Power chain structure

Several configurations of power chain are shown in the literature. We cite as examples:
- The four-engine wheels configuration to direct mechanical linkage or gears.
- The configuration with two motors front or rear to direct connection or with gear.
- The single-engine configuration with mechanical differential transmission more gears or gearless. This configuration is chosen for our application because it offers the advantage of low cost, because the manufacture of a single motor is less expensive than many engines. This configuration also avoids the problem of slippage since it is impossible to control several motors at the same speed.

The power chain structure is illustrated by the figure 1.

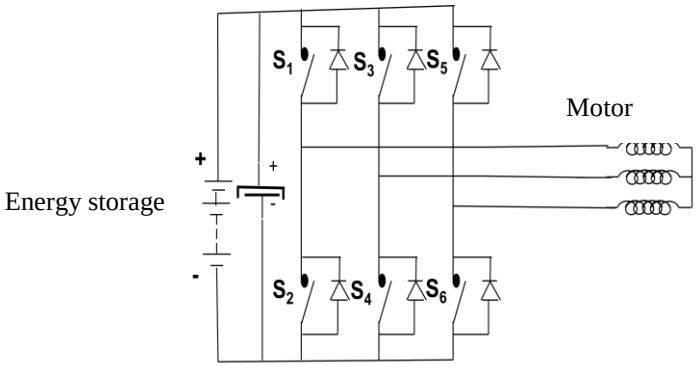

Fig.1. Power chain structure

Usually the static converter is with IGBTs. In our case we have replaced the transistor IGBT by electromagnetic switch to push the multiple disadvantages of IGBTs.
During the phases of acceleration and constant speed operation, the motor is driven by the power converter with electromagnetic switch according to the scalar control strategy imposing the motor phase current in phase with the electromotive force, leading to a minimization of energy consumption [1], [2].

2.1. Converter structure

The static converter is a two-level inverter voltage. This structure is the least expensive compared to others and offers good quality of voltages and currents wave-forms, which leads to a good dynamic characteristic of EVs. Two inverter types are studied, the IGBT converter structure and the electromagnetic switches converter structure. The latter structure has the disadvantage of low switching frequency (Below 150 Hz), but it is less expensive and does not pose the problem of floating potential, since each inverter arm is controlled by a single electro-magnet. Against, the IGBT structure offers the possibility to achieve a switching frequency of 8000 Hz which leads to a good quality of the dynamic characteristic of EVs, it present a lot of disadvantages which can be cited as examples :

- Energy losses leading to a reduced range for a stored energy also establishes the temperature rise in the transistors and diodes leading to the incorporation of a cooling system in most cases.
- The problem of potential-floating leading to a complication of the electronic control circuit.
- The intervention of capacity Trigger-emitter, Trigger-collector and Collector-emitter. These capacities occur especially at high frequencies leading to a deterioration of the quality of control signals and subsequently to performance degradation of the overall drive system
- The problem of static and dynamic Luch-up generally leading to the deterioration of the converter. In this paper we only present the design process of the converter with electromagnetic switches. Design methods of the IGBT inverter are highly processed and presented in the literature [3].

The design parameters of the generator coil are shown in figure 2.

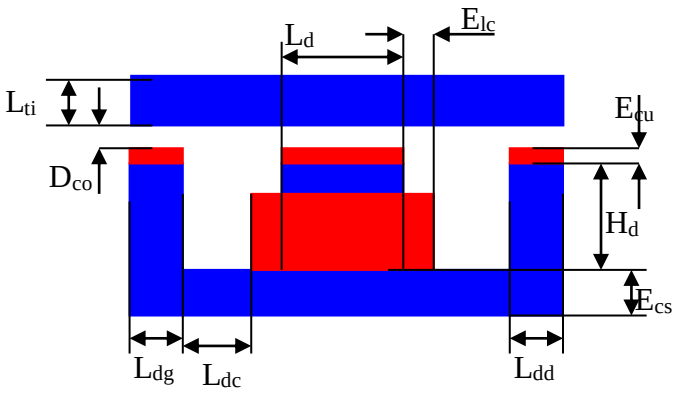

Fig.2. Design parameters of the generator coil

For the electromagnetic switches converter structure, the electromagnet is a modular structure. Indeed, several modules can be stacked either in series or in parallel to increase the attraction force, and thereafter the opening and closing frequency of the contacts of the static converter.

The stack in parallel has the advantage that the frequency of closing and opening of the switches is clearly higher in regard to the stack in series structure, because these actions are performed by action of the attraction force of two generator coils.

The parallel stack of two modules is illustrated in figure 3 [3].

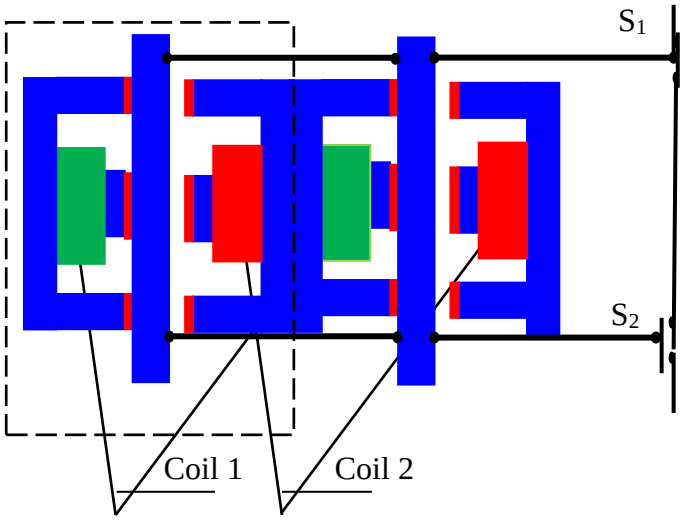

Fig.3. Stacking in parallel of two modules

The equation of movement of the stem is deducted from the fundamental relation of the dynamics [3]:

$$nmp \times M_t \times \frac{dv}{dt} = nmp \times \frac{\mu_0 \times \mu_r}{4} \times \frac{I^2 \times N_{sb}^2}{(E_{cu} + D_{co} - X_t)^2} \quad (1)$$

$$v = \frac{dx_t}{dt} \quad (2)$$

Where v and M_t are respectively the velocity and the mass of the moving rod, nmp is the number of modules, N_{sb} is the spires number of the generating coil, E_{cs} is the thickness of the copper layer, D_{co} is the opening of the movable stem, x_t displacement of the mobile stem and μ_r is the relative permeability of copper.

This structure presents the time of opening and the one of closing weakest, since closing and opening of the power contacts take place joint-stock of two generating coils. The increase of the number of module increases the frequency of closing and opening of contacts, what brought us to choose only one module to push the problem of increase of the cost of the structure, slightly.

For only one module, the time of closing and opening is estimated to:

$T_{on}=T_{off}$ = 3.74 e-3 s

From where the frequency of closing and to the opening is estimated to:

$$F_{ri} = \frac{1}{T_{on}+T_{off}} = \frac{1}{2\times 3.74e-3} = 133.7\ hz \quad (3)$$

In conclusion, the structure to parallel stacking with only one module is chosen for the continuation of survey.

2.2. Sizing of the electric motor

The selected structure of the engine is with permanent magnet and axial flux. This structure is built with the same radius for the stator and the rotor. The slots directed towards the motor's center. The magnets shape is the same than the main teeth. This structure is with reduced production cost and high power to weight ratio.

A configuration to 5 pairs of poles and 6 main teeth is illustrated by the figure 4:

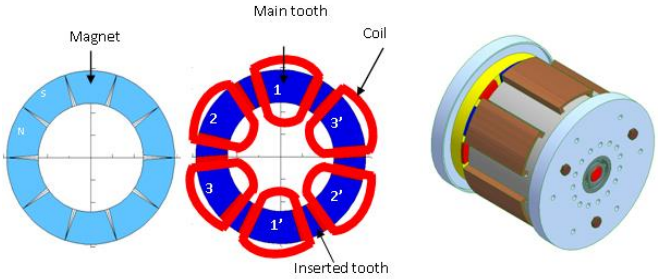

Fig.4. Configuration to 5 pairs of poles and 6 main teeth

The magnetic induction in the air gap is calculated for a position of maximum overlap, since this position is relative to the maximum induction in the different active parts of the stator magnetic pole of the motor. The distribution of the field lines to this position is illustrated by figure 5.

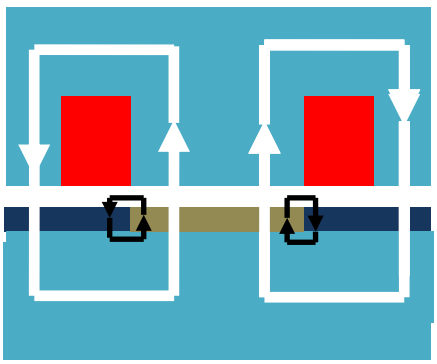

Fig.5. Distribution of the field lines to a position of maximum recovery

This figure shows that the flux is divided into useful flux for the traction of the rotor and leakage flux between the magnets.

Applying Ampere's theorem at stator pole to a supply of the stator coil by the maximum current of the motor, regardless of the magnetic flux due to the magnets, used to calculate the magnetic induction caused by the current [1], [10], [11], [12], [13], [14], [15].

$$\int_{\text{Filed lines}} \vec{H}\times\vec{dl} = \frac{N_s}{\frac{N_d}{3}}\times I_{max} = 2\times\left(H_{ri}\times H_a + H_{ri}\times e\right) \quad (4)$$

Where I_{max} is the maximal current of the motor, H is the magnetic field, H_{ri} is the magnetic field in the air-gap, H_a is the height of a magnet, e is the thickness of the air-gap, μ_0 is the permeability of air, N_s is the number of spires by phase and N_d is the number of main teeth [1], [2].

$$B_{ri} = \mu_0 \times H_{ri} \quad (5)$$

Where B_{ri} is the magnetic induction due to the energize of the motor by the maximal current (I_{max}) [1], [2]:

$$B_{ri} = \frac{\mu_0}{2\times\frac{N_d}{3}} \times \frac{N_s \times I_{max}}{H_a + e} \quad (6)$$

This induction is negligible compared to the induction created by the magnets, since the flux generated by the coil through two times the thickness of the magnets and the air gap having both a very low magnetic permeability. Accordingly, only the magnetic flux generated by the magnets is used for sizing the motor.

This induction is derived from the application of Ampere law on a closed contour of the field lines:

$$\int_{\text{Filed lines}} \vec{H}\times\vec{dl} = 0 = 2\times\left(H_m\times H_a + H_e\times e\right) \quad (7)$$

Where H_m and H_e are respectively the magnet magnetic filed and the air-gap magnetic filed.

The magnetic induction in the air gap is linear in function of the magnetic field in the gap:

$$B_e = \mu_0 \times H_e \quad (8)$$

While applying the theorem of conservation of flux to the level of the air-gap, we deducts the expression of the induction in the entrefer according to the induction in the magnets and the coefficient of leakage flux:

$$B_a \times S_a \times K_{fu} = B_e \times S_d \quad (9)$$

Where S_a and S_d are respectively the magnet and the stator tooth sections.

The magnetic induction of the magnets takes the following relation:

$$B_a = \frac{S_d}{S_a} \times \frac{B_e}{K_{fu}} \quad (10)$$

Where K_{fu} is the coefficient of flux leakages.

The induction in the magnets is approached by the following linear equation:

$$B_a = \mu_0 \times \mu_r \times H_m + B_r \quad (11)$$

Where μ_r is the relative permeability of the magnets and B_r is the residual magnetic induction of magnets.

From the equations (7), (8), (9), (10) and (11), we deducts the height of the magnets imposing an induction in the air-gap B_e. This induction is chosen of a manner to have magnetic inductions in the different active parts of the motor near of the bends saturation of the characteristic B-H, leading to a minimal mass of the motor and a working in the linear regime [1]:

$$H_a = \mu_r \times \frac{B_e}{B_r - \frac{S_d \times B_e}{S_a \times K_{fu}}} \times e \quad (12)$$

To avoid the demagnetization of the magnets, the current of phase must be lower than demagnetization current Id [10]:

$$I_d = \left(\frac{B_r - B_c}{\mu_r} \times H_a - B_c \times K_{fu} \times e \right) \times \frac{p}{2 \times \mu_0 \times N_s} \quad (13)$$

Where B_c is the demagnetization induction, B_r is the residual induction of magnets, μ_0 is the permeability of air and p is number of poles pairs.

3. Modeling of the electrical Parameters of the power chain

3.1 Phase inductance of the motor

The inductance of this motor structure, for operation in linear mode is constant since the magnets are planar. To calculate the phase inductance of the motor, the magnets are replaced with air, since their relative permeability is very close to that of a vacuum, and the motor is energized by maximal current. The figure 6 illustrates the distribution of the field lines to the level of a stator pole.

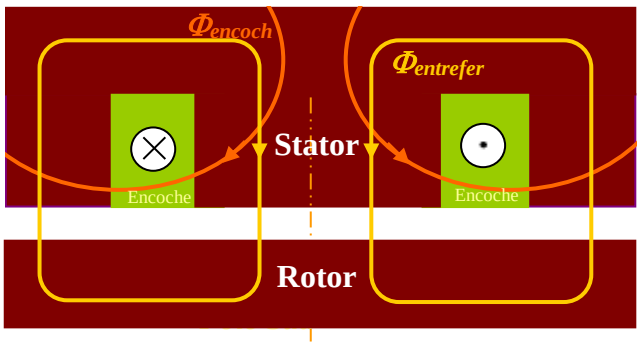

Fig.6. Distribution of the field lines for a powered coil

This figure shows the presence of a flux leakages passing through the slot opening in a presence of leakage inductance in the slots copper, and of a main flux passing twice through the air gap and the magnet giving presence to an inductance of gap.

We recall the equations to model an inductance for a linear system:

$$L \times i_1 = N_s \times \emptyset_1 \quad (14)$$

$$R \times \emptyset_1 = N_s \times i_1 \quad (15)$$

$$L = \frac{N_s^2}{R} \quad (16)$$

Where L is the inductance, i_1 is the current of energize, N_s is the number of spire and Φ_1 is the flux giving birth to the L inductance and $\Re$ is the reluctance of the magnetic circuit.

The figure 7 illustrates the network of reluctance modeling the inductance of total phase of the motor.

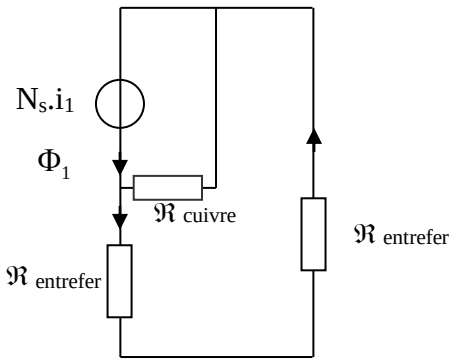

Fig.7. Network reluctance modeling inductance

According to this face, we can write:

$$N_s \times i_1 = (2 \times R_{entrefer}) \times \emptyset_{entrefer} \times R_{cuivre} \times \emptyset_{encoche} \quad (17)$$

With the reluctance of the air gap and the copper are given by the following relationship:

$$R_{entrefer} = \frac{1}{\mu_0} \times \frac{(e + H_d)}{S_d/2} \quad (18)$$

$$R_{cuivrer} = \frac{1}{\mu_0} \times \frac{(L_{enc})}{\left(\frac{D_e - D_i}{2} \times H_d\right)} \quad (19)$$

The leakage flux through the copper through about half of the copper surface from which the occurrence of the coefficient 2 in calculating of the reluctance of the leakage flux in the copper. The value of the total inductance is deduced from equations (17), (18) and

(19):

$$L = L_{fuite} + L_{entrefer} = \frac{N_s^2}{R_{cuivre}} + \frac{N_s^2}{2+R_{entrefer}} \quad (20)$$

$$L = 2 \times \frac{\mu_0}{4} \times \left(\frac{S_d/2}{2\times(e+H_a)} + \frac{\left(\frac{D_e-D_i}{2}\right)\times H_d}{L_{enc}} \right) \times N_s^2 \quad (21)$$

Where S_d is the section of the main tooth, H_d is the height of the slot, H_a is the height of the magnet, L_{enc} is the width of the slot, e is the thickness of the air-gapr and $\Re$ is the reluctance.

3.2 Mutual inductance of the motor

The principle of the calculation of the mutual inductance is based on the supply of a coil for the calculation of the flux sensed by the adjacent coil. The flux path determines the total reluctance of the magnetic circuit modeling this mutual inductance. Figure 8 shows the trajectory of the flux:

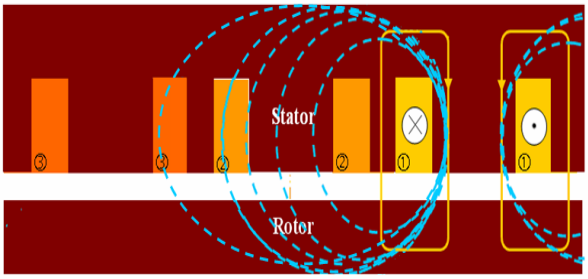

Fig.8. Distribution of the flux generated by the coil powered and captured by the adjacent coils

From Figure 9 we deduce that the reluctance network modeling the mutual inductance.

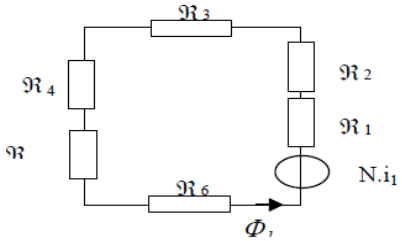

Fig.9. Reluctance network modeling the mutual inductance

Where $\Re_1$ is the reluctance of the air-gap in front of the tooth where the coil 1 is accommodated, $\Re_2$ is the reluctance of a major tooth, $\Re_3$ is the reluctance of the stator yoke, $\Re_4$ is the reluctance of the tooth where coil 2 is housed, $\Re_5$ is the reluctance of the air-gap in front of tooth 2 and $\Re_6$ is the reluctance of the rotor yoke. The expression of the mutual inductance is given by:

$$M_{12} \times i_1 = N_s \times \emptyset_1 \quad (22)$$

$$M_{12} = \frac{N_s^2}{\Re} \quad (23)$$

Where Φ_1 is the flux sensed by the coil 2 by supplying the coil 1 and $\Re$ is the total reluctance. Different mutual inductances of the motor are equal since the engine is symmetrical.

$$R_1 = \frac{1}{\mu_0} \times \frac{2\times(e+H_e)}{sd} \quad (24)$$

$$R_2 = \frac{1}{\mu_0} \times \frac{2\times H_d}{S_d} \quad (25)$$

$$R_3 = \frac{1}{\mu_0\times\mu_r} \times \frac{\left(2\times A_{encm}+\frac{1}{2}\times A_{dentm}+A_{dentim}\right)\times\left(\frac{D_e+D_i}{4}\right)}{H_{cs}\times\left(\frac{D_e-D_i}{2}\right)} \quad (26)$$

$$R_4 = \frac{1}{\mu_0} \times \frac{2\times H_d}{S_d} \quad (27)$$

$$R_5 = \frac{1}{\mu_0} \times \frac{2\times(e+H_e)}{sd} \quad (28)$$

$$R_6 = \frac{1}{\mu_0\times\mu_r} \times \frac{2\times\left(2\times A_{encm}+\frac{1}{2}\times A_{dentm}+A_{dentm}\right)\times\frac{D_e+D_i}{4}}{H_{cr}\times\left(\frac{D_e-D_i}{2}\right)} \quad (29)$$

A_{encm} where is the average width of the slot, A_{dentm} is the average width of the main tooth, A_{dentim} is the average width of the tooth interposed, H_{cr} is the height of the rotor yoke, H_{cs} is the height of the stator yoke, μ_0 is the absolute permeability, μ_r is the relative permeability of the magnets. We deduce a general expression for the mutual inductance of the motor:

$$M_{12} = \frac{N_s^2}{2\times(R_1+R_2+R_3+R_4+R_5+R_6)} \quad (30)$$

3.3 Electro-magnet inductance

The trajectory of the flux when supplying the coil is shown in figure 10.
Hence, we deduce the reluctance network modeling the coil (Figure 10).

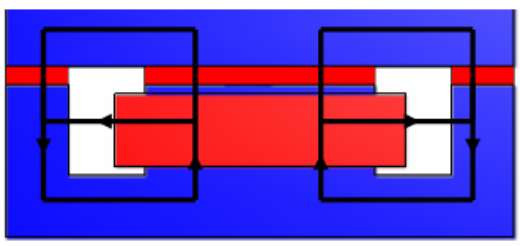

a. Trajectory of the flux

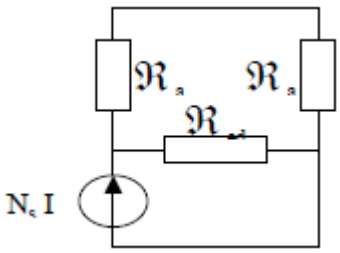

b. Reluctance network

Fig.10. Trajectory of the flux and reluctance network modeling the coil

Where $\mathfrak{R}_a$ is the reluctance of the air-gap and $\mathfrak{R}_{ed}$ is the reluctance of the space between tooth. From the network reluctance above, we deduce the expression of the inductance of the generating coil:

$$L_b = \frac{N_{sb}^2}{2 \times R_a} + \frac{N_{sb}^2}{R_{ed}} \quad (31)$$

$$R_a = \frac{1}{\mu_0} \times \frac{E_{cu} + D_{co} - X_t}{\frac{S_d}{2}} \quad (32)$$

Where D_{co} is the maximum aperture of the rod, X_t is the displacement of the rod, D_{co} is the maximum aperture of the rod and $\boldsymbol{X_t}$ is the displacement of the rod.

$$R_{ed} = \frac{1}{\mu_0} \times \frac{E_{lc} + L_{dc}}{H_{cu} \times E_b} \quad (33)$$

Where H_{cu} is the height of the coil and L_{dc} is the distance between the coil and the right tooth. Hence, we deduce the expression of the inductance of the coil:

$$L_b = \mu_0 \times N_{sb}^2 \left(\frac{\frac{S_d}{2}}{2 \times E_{cu} + D_{co} - X_t} \right) + \frac{H_{cu} \times E_b}{E_{lc} + L_{dc}} \quad (34)$$

3.4 Attraction force of the electromagnet

The attraction force of the rod derives from the energy stored in the coil:

$$W_b = \frac{1}{2} \times L_b \times I^2 \quad (35)$$

$$F = \frac{\mu_0 \times \mu_r}{4} \times \frac{I^2 \times N_{sb}^2}{(E_{cu} + D_{co} - X_t)^2} \quad (36)$$

3.5 DC-bus voltage

The DC bus voltage is calculated in such a way that the vehicle can reach a maximum speed with a low torque undulation and without weakening. This voltage is calculated assuming that the engine runs at a stabilized maximum speed. At this operating point the electromagnetic torque to be developed by the motor is expressed by the following equation:

$$T_{Udc} = \frac{P_f}{\Omega_{max}} + T_d + (T_b + T_{vb} + T_{fr}) + \frac{T_r + T_{a+Tc}}{r_d} \quad (37)$$

Where P_f are the iron losses, T_d is the torque losses in the gear and Ω_{max} is the maximum angular speed. The different torques are expressed by the following equations:

$$T_b = S \times \frac{V}{|V|} \quad (38)$$

$$T_{vb} = \aleph \times V \quad (39)$$

$$T_{fr} = K \times V \times |V| \quad (40)$$

$$T_r = R_w \times f_r \times M_v \times g \quad (41)$$

$$T_a = R_w \times \frac{(M_{va} \times C_x \times A_f)}{2} \times V^2 \quad (42)$$

$$T_c = M_v \times g \times \sin(\lambda) \quad (43)$$

Where s is the dry friction coefficient, χ is the viscous friction coefficient, k is the fluid friction coefficient, λ is the angle that the road makes with the horizontal, M_{va} is the density of the air, C_x is the aerodynamic drag coefficient and A_f is the vehicle frontal area.

At this operating point, the phase current of the motor is expressed by the following equation:

$$I_p = \frac{T_{Udc}}{K_e} \quad (44)$$

The converter's continuous voltage for sinusoidal control is expressed as follow [4]:

$$U_{dc} = \frac{\pi}{2} \times \sqrt{\left(R \times I_p + E_{phi}\right)^2 + \left(L \times p \times \Omega_{max} + I_p\right)^2} \quad (45)$$

E_{phi} is the maximal value of electromotive force.

$$E_{phi} = \frac{2}{3} \times K_e \times \Omega_{max} \quad (46)$$

3.6 Gear ratio

The insertion of a gear speed reducer with rd ratio aims to enable the vehicle to reach the maximum speed of 80 km / h in our application. This ratio also helps ensure proper interpolation of reference voltages in order to have a good quality of electromagnetic torque.

$$r_d = \frac{2 \times \pi \times R_w \quad \times F_{ri}}{n_{qTA} \times V_{max} \times p \times n_{iTR}} \quad (47)$$

Where n_{iTR} is the reference voltages interpolation coefficient, V_{max} is the vehicle maximal velocity, n_{qTA} is the coefficient of quality of the supplying voltage, F_{ri} is the switching frequency and R_w is the vehicle wheel radius.

4. Motor-converter model

The engine is powered by a voltage inverter at two levels. IGBT transistors are replaced by ideal electromagnetic switches, to reduce losses and sink multiple disadvantages of IGBTs, such as:

- Tail current.
- The problem of floating mass leading to a complication of the control circuit.
- Static and dynamic Luch-up phenomenon leading to a deterioration of the converter in the majority of cases.
- Switching and conduction losses significant.
- Heat IGBT transistors, leading to the need for the integration of a cooling system in the most cases.

Each phase of the motor is equivalent to a resistor in series with an inductance and a back electromotive force. The model of the three phases is described by the following equations [4], [5]:

$$u_1 = R \times i_1 + (L - M) \times \frac{di_1}{dt} + \frac{2}{3} \times k_e \times \Omega \times \cos\left(p \times \Omega \times t + \frac{\pi}{2}\right) \quad (48)$$

$$u2 = R \times i_1 + (L - M) \times \frac{di_2}{dt} + \frac{2}{3} \times k_e \times \Omega \times \cos\left(p \times \Omega \times t - \frac{2 \times \pi}{3} + \frac{\pi}{2}\right) \quad (49)$$

$$u_3 = R \times i_3 + (L - M) \times \frac{di_3}{dt} + \frac{2}{3} \times k_e \times \Omega \times \cos\left(p \times \Omega \times t - \frac{4 \times \pi}{3} + \frac{\pi}{2}\right) \quad (50)$$

Where R, L, M and Ke are respectively the resistance, inductance, mutual inductance and the electric motor constant, ii is the current of the phase i and ui is the i phase voltage.

The electromagnetic torque is given by the following relationship:

$$T_{en} = \frac{1}{\Omega}(e_1 \times i_1 + e_2 \times i_2 + e_3 \times i_3) \quad (51)$$

Where e_i is the electromotive force of the phase i. The model of the motor-converter is implanted under the Matlab-Simulink environment according to the following block diagram:

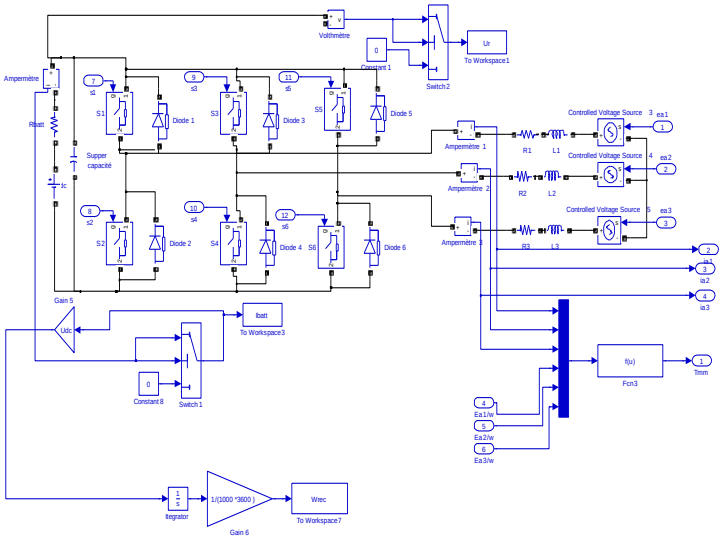

Fig.11. Simulink model of the motor-converter

5. Speed regulator

The comparison of the reference speed and the response speed provides the amplitude of the reference currents minimizing the error between the reference speed and the speed of response. Indeed, the reference speed is compared to the response speed. The comparator attacks a proportional-integral-type (PI regulator) to provide the amplitude of reference currents minimizing the speed error. The Simulink model of speed regulator is illustrated by the figure 12

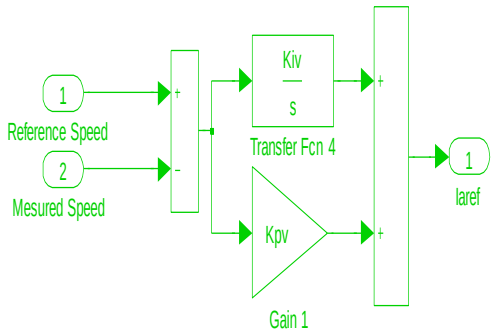

Fig.12. Simulink model of the speed regulator

6. Currents regulators

Current regulators impose currents having the same shape and in phase with the electromotive forces against. Indeed, the reference currents are compared to the phase currents of the motor. The outputs of the three comparators attack three regulators proportional integral-type / (PI) to provide three voltages necessary to impose ideal reference current in phase with the electromotive forces against and to minimize the error between the reference speed and response speed of the electric vehicle. The Simulink model of currents regulators is shown in figure 13:

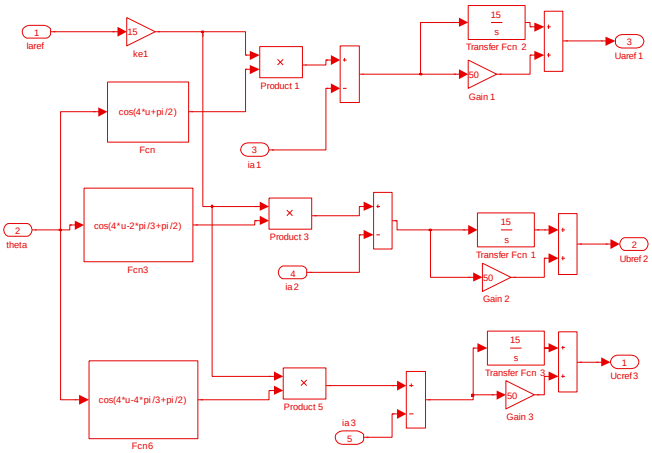

Fig.13. Simulink model of currents regulators

7. Model of the back electromotive forces

The three back electromotive forces are reconciled by the following three equations:

$$e_1 = \frac{2}{3} \times k_e \times \Omega \times \cos\left(p \times \Omega \times t + \frac{\pi}{2}\right) \quad (52)$$

$$e_2 = \frac{2}{3} \times k_e \times \Omega \times \cos\left(p \times \Omega \times t - \frac{2\times\pi}{3} + \frac{\pi}{2}\right) \quad (53)$$

$$e_3 = \frac{2}{3} \times k_e \times \Omega \times \cos\left(p \times \Omega \times t - \frac{4\times\pi}{3} + \frac{\pi}{2}\right) \quad (54)$$

These equations are implemented under the Matlab-Simulink environment according to the following block diagram:

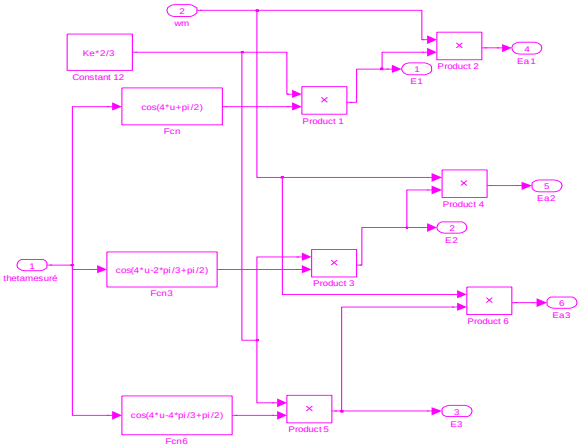

Fig.14. Model Simulink of the back electromotive forces

8. Control signals generator

The control signal generator compares the three reference voltages to a triangular signal with frequency significantly higher than the frequency of the voltages provided by the currents regulators. The output of each comparator attack an hysteresis variant between 0 and 1 for outputting the signals for controlling the switches S1 , S3 and S5 . The speed controller and current controller adjusts the pulse width of the control signals so as to impose currents in phase with the electromotive forces against and minimize the error between the reference speed and the speed of response. Signals for controlling the switches S2, S4 and S6 are respectively complementary to the signals S1, S3 and S5. To prevent short circuits, control pulses S2, S4 and S6 are shortened to avoid duplication between two signals control arm. The Simulink model of the generator control signals is shown in figure 15:

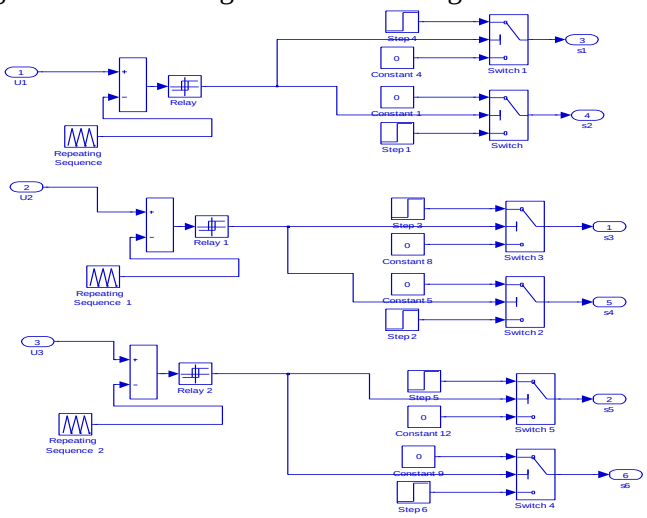

Fig.15. Simulink model of control signals generator

9. Dynamic equation

The dynamic equation of the vehicle is derived from the fundamental relationship of dynamics:

$$(M_v \times R_r) \times \frac{dv}{dt} = r_d \times T_m - (F_r + F_a + F_c) \times R_r \qquad (55)$$

Where F_r is the rolling resistance force, F_a is the aerodynamic force and F_c is the force of gravity.
Where :

$$F_r = f_r \times M_v \times g \qquad (56)$$

$$F_a = \frac{1}{2} \times M_{va} \times C_x \times S_f \times V^2 \qquad (57)$$

$$Fc = Mv \times g \times \sin(\lambda) \qquad (58)$$

The equation of motion of the vehicle is implemented under the environment of Matlab/ Simulink as shown in to the figure 16:

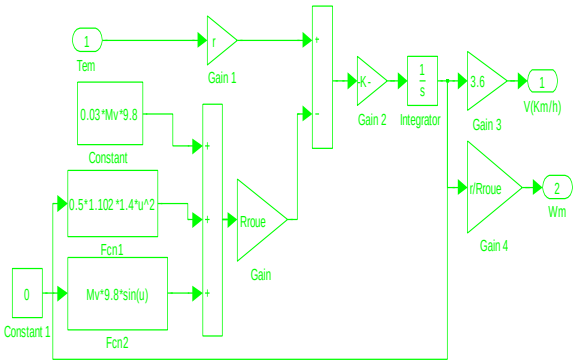

Fig.16. Simulink model of the dynamic equation

10. Global model of the power chain

The coupling of different models of the electric vehicle power chain leads to overall model implemented under the environment of Matlab/ Simulink as shown in to the figure 17:

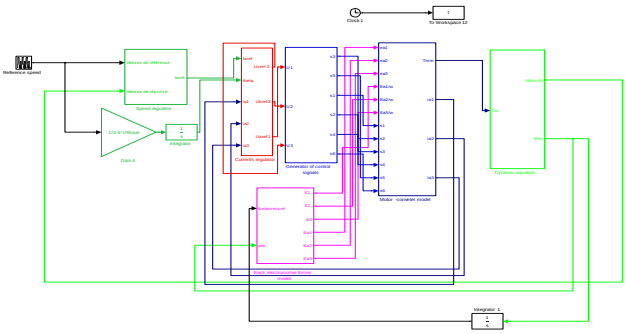

Fig.17. Global model of the power chain

11. Descriptions of the simulations results

Scalar control has the disadvantage of convergence at startup, but for the electric car application, the acceleration during start-up is reduced to avoid the problem of abrupt starting and to increase the reliability of the vehicle. This property makes it very robust the scalar control for electric car application. This feature is illustrated in Figure 18. Also this figure shows that the speed of response precisely follows the reference speed, which shows the performance of the control technique chosen. This characteristic validates design process of the power chain.

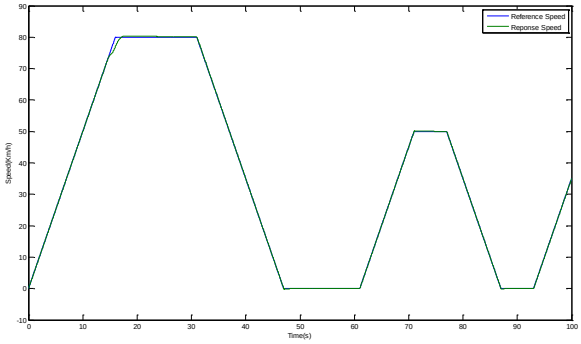

Fig.18. Speed response

Figure 19 shows that the starting current is significantly reduced, which shows the good choice of the parameters of speed and currents regulators.

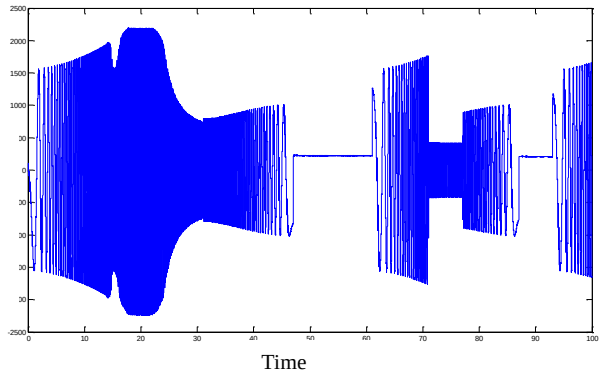

Fig.19. Phase current

Figure 20 shows that the torque on the motor shaft is negative during deceleration, since the inertia of the drive power is negative.

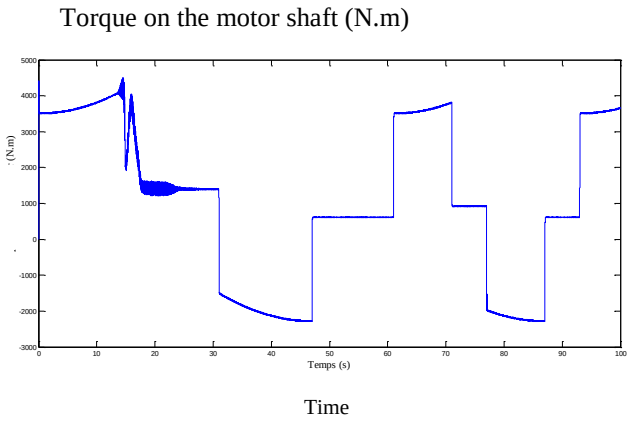

Fig.20. Torque on the motor shaft

The electric car recovers energy hang deceleration phases. This property is illustrated by figure 21.

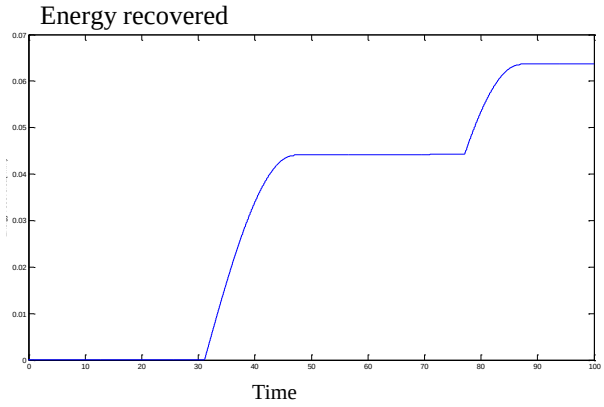

Fig.21. Energy recovered

The control law imposes a phase shift ideally zero to minimize consumption, but in reality this phase shift is close to zero since the time constant of the motor is not zero. This property is illustrated by figure 22:

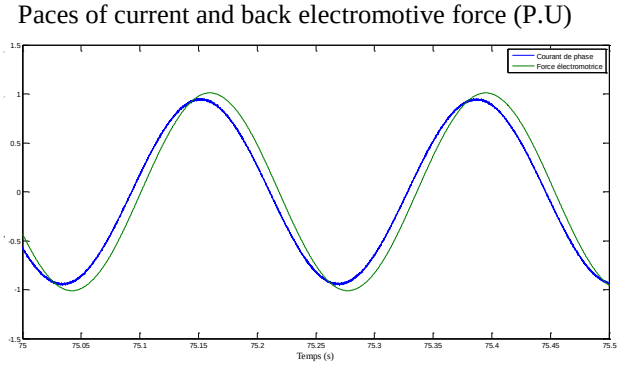

Fig. 22. Paces of current and back electromotive force

This figure shows that the shape of the current is very close to sinusoïdal shape, which shows the effectiveness of the selected control law.

12. Conclusion

In this paper we present a systemic scalar control and design methodology of the traction chain of electric vehicles. This methodology takes into account the interactions between the control and the design of the motor-converter. The system modeling along with a sinusoidal control law under the environment of Matlab / Simulink, validates this design approach and leads to a scientific results to good level.

References

[1] S. TOUNSI, «Modélisation et optimisation de la motorisation et de l'autonomie d'un véhicule électrique», Thèse de Doctorat 2006, ENI Sfax.

[2] S. TOUNSI et R. NEJI: «Design of an Axial Flux Brushless DC Motor with Concentrated Winding for Electric Vehicles», Journal of Electrical Engineering (JEE), Volume 10, 2010 - Edition: 2, pp. 134-146.

[3] S. TOUNSI, M. HADJ KACEM et R. NEJI « Design of Static Converter for Electric Traction », International Review on Modelling and Similations (IREMOS) Volume 3, N. 6, December 2010, pp. 1189-1195.

[4] R. NEJI, S. TOUNSI et F. SELLAMI: «Contribution to the definition of a permanent magnet motor with reduced production cost for the electrical vehicle propulsion», European Transactions on Electrical Power (ETEP), 2006, 16: pp. 437-460.

[5] R. NEJI, S. TOUNSI, F. SELLAMI: «Optimization and Design for a Radial Flux Permane otor for Electric Vehicle», Journal (Systems, Volume 1, isuue 4 (2005), pp. 47-68.

[6] Chaithongsuk, S., Nahid-Mobarakeh, B., Caron, J., Takorabet, N., & Meibody-Tabar, F. : Optimal design of permanent magnet motors to improve field-weakening performances in variable speed drives. Industrial Electronics, IEEE Transactions on, vol 59 no 6, p. 2484-2494, 2012.

[7] Rahman, M. A., Osheiba, A. M., Kurihara, K., Jabbar, M. A., Ping, H. W., Wang, K., & Zubayer, H. M. : Advances on single-phase line-start high efficiency interior permanent magnet motors. Industrial Electronics, IEEE

Transactions on, vol 59 no 3, p. 1333-1345, 2012.
[8] El-Refaie, A. M. : Fractional-slot concentrated-windings synchronous permanent magnet machines: Opportunities and challenges. Industrial Electronics, IEEE Transactions on, vol 57 no 1, p. 107-121, 2010.
[9] Dorrell, D. G., Hsieh, M., Popescu, M., Evans, L., Staton, D. A., & Grout, V. : A review of the design issues and techniques for radial-flux brushless surface and internal rare-earth permanent-magnet motors. Industrial Electronics, IEEE Transactions on, vol 58 no 9, 3741-3757, 2011.
[10] Parasiliti, F., Villani, M., Lucidi, S., & Rinaldi, F. : Finite-element-based multiobjective design optimization procedure of interior permanent magnet synchronous motors for wide constant-power region operation. Industrial Electronics, IEEE Transactions on, vol 59 no 6, p. 2503-2514, 2012.
[11] Mahmoudi, A., Kahourzade, S., Rahim, N. A., & Ping, H. W. : Improvement to performance of solid-rotor-ringed line-start axial-flux permanent-magnet motor. Progress In Electromagnetics Research, 124, p. 383-404, 2012.
[12] Duan, Y., & Ionel, D. M. : A review of recent developments in electrical machine design optimization methods with a permanent-magnet synchronous motor benchmark study. Industry Applications, IEEE Transactions on, vol 49 no 3, p. 1268-1275, 2013.
[13] Islam, M. S., Islam, R., & Sebastian, T. : Experimental verification of design techniques of permanent-magnet synchronous motors for low-torque-ripple applications. Industry Applications, IEEE Transactions on, vol 47 no 1, p. 88-95, 2011.
[14] Liu, G., Yang, J., Zhao, W., Ji, J., Chen, Q., & Gong, W. : Design and analysis of a new fault-tolerant permanent-magnet vernier machine for electric vehicles. Magnetics, IEEE Transactions on, vol 48 no 11, p. 4176-4179, 2012.
[15] Lee, S., Kim, K., Cho, S., Jang, J., Lee, T., & Hong, J. : Optimal design of interior permanent magnet synchronous motor considering the manufacturing tolerances using Taguchi robust design. Electric Power Applications, IET, vol 8 no 1, 23-28, 2014.